Complex Oscillations and Chaos in Electrostatic Microelectromechanical Systems under Superharmonic Excitations

Sudipto K. De and N. R. Aluru*

Department of Mechanical and Industrial Engineering Beckman Institute for Advanced Science and Technology, University of Illinois at Urbana-Champaign, Urbana, Illinois, USA

(Received 2 November 2004; published 26 May 2005)

In this Letter, the formation of complex oscillations of the type $2^n M$ oscillations per period at the Mth superharmonic excitation is reported for electrostatic microelectromechanical systems. A dc bias (beyond "dc symmetry breaking") and an ac signal (at the Mth superharmonic frequency) with an amplitude around "ac symmetry breaking" gives rise to M oscillations per period or period M response. On increasing the ac voltage, a cascade of period doubling bifurcations take place giving rise to $2^n M$ oscillations per period. An interesting chaotic transition (1-band and 2-band chaos) is observed during the first period doubling bifurcation. The nonlinear nature of the electrostatic force is shown to be responsible for the reported observations.

DOI: 10.1103/PhysRevLett.94.204101 PACS numbers: 85.85.+j, 05.45.Pq

Nonlinearities in microelectromechanical systems (MEMS) can arise from various sources such as spring and damping mechanisms [1], resistive, inductive, and capacitive circuit elements [2], and surface, fluid, electrostatic, and magnetic forces [3]. Nonlinear dynamic phenomena like spring hardening or softening, jump phenomenon, hysteresis [4], and period doubling route to chaos at resonant excitation [3,5] have been observed in electrostatic MEMS. In this Letter, new nonlinear dynamic properties of electrostatic MEMS under superharmonic excitations are presented.

Dynamic analysis of electrostatic MEMS requires the coupled solution of the electrical, fluidic, and mechanical equations. In the absence of any free charges, from Gauss's law, the Laplace equation is obtained which is solved for the electrostatic potential [6], i.e.,

$$\nabla^2 \phi = 0 \quad \text{in } \Omega, \tag{1}$$

where ϕ is the potential field in the dielectric medium Ω (air in this case) surrounding the conductors and electrodes. A boundary integral formulation (see [7] for details) of Eq. (1) is used to compute the surface charge density σ on the conductors. The electrostatic pressure P_e acting on the microstructure can be computed from σ as $P_e = \sigma^2/2\epsilon$, where ϵ is the permittivity of air. Air damping between the MEM structure and the ground electrode is modeled using squeeze film damping. Considering compressible slip flow, the isothermal Reynolds squeeze film equation can be written as (see [8] for details)

$$\nabla \cdot ((1 + 6K)h^3 P_f \nabla P_f) = 12\eta \frac{\partial (P_f h)}{\partial t}, \tag{2}$$

where h is the gap between the MEM structure and the ground electrode, P_f is the air pressure, and η is the air viscosity. $K = \lambda/h$ is the Knudsen number and λ is the mean free path of air. Equation (2) is obtained (see [8] for details) from the Navier-Stokes equation by accounting for the slip correction and by neglecting the fluid velocity and the variations of all physical quantities in the height direction.

The mechanical deformation of the MEM structure due to the electrostatic and fluidic forces is obtained by performing transient 2D large deformation elastic analysis of the microstructure (see [9] for details)

$$\rho \ddot{\mathbf{u}} - \nabla \cdot (\mathbf{FS}) = 0, \tag{3}$$

where ρ is the material density, $\ddot{\mathbf{u}}$ is the acceleration vector, $\mathbf{F}$ is the deformation gradient, and $\mathbf{S}$ is the second Piola-Kirchhoff stress. The inertial force is counterbalanced by the restoring force due to structural stiffness in the absence of any body forces and material damping within the structure. Appropriate displacement and surface traction bound-

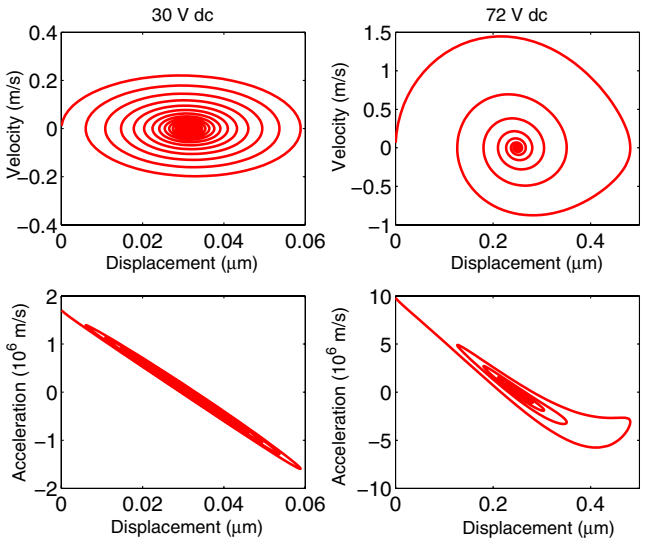

FIG. 1 (color online). dc symmetry breaking in x-$\dot{x}$ phase plot and corresponding bending in x-$\ddot{x}$ phase plot differentiating linear (30 V dc) and nonlinear state (72 V dc).

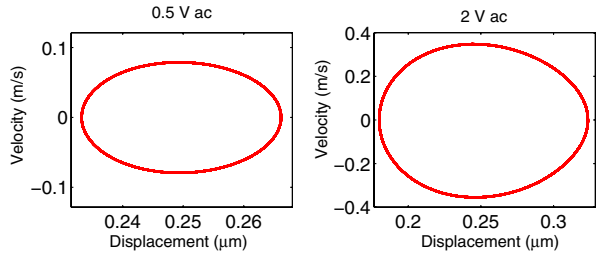

FIG. 2 (color online). ac symmetry breaking in x-$\dot{x}$ phase plot for 72 V dc bias.

ary conditions (from electrostatic and fluid damping analysis) are applied. Equations (1)–(3) are solved in a self-consistent manner [9] and are termed as full scale simulations in this Letter.

A 80 μm $\times$ 1 μm $\times$ 10 μm (length $\times$ height $\times$ width) Si fixed-fixed beam MEM device, 1 μm over a ground plane is considered (see [9] for more details on the geometry of the MEM device). The dynamic pull-in voltage of the microstructure is 73 V. The microstructure is first brought to a steady nonlinear state by applying a dc voltage close to the dynamic pull-in voltage. Symmetry breaking [10] in the x-$\dot{x}$ phase plot or bending in the x-$\ddot{x}$ is a good indicator of this nonlinearity as shown in Fig. 1. No symmetry breaking (spirals inward in a symmetric fashion) or bending (spirals inward following a straight line) is observed at small dc voltages (e.g., 30 V) indicating a linear state. On the other hand, when the dc voltage is close to the pull-in voltage (e.g., larger than 69 V dc), the system exhibits symmetry breaking and bending. This symmetry breaking is termed as dc symmetry breaking in this Letter.

Once the microstructure reaches a stable nonlinear state, it is excited with an ac voltage (V_{ac}) with a frequency f_0/M, where f_0 is the resonant frequency of the microstructure at the applied dc bias and M is a natural number. For small values of V_{ac}, normal one oscillation per period is observed for all M. As V_{ac} is increased, a second symmetry breaking, termed as the ac symmetry breaking, is observed as shown in Fig. 2 for a 72 V dc bias ($f_0 = 0.763$ MHz) and $M = 1$. A small ac voltage (e.g., 0.5 V ac) does not show any symmetry breaking (elliptical shape), whereas an ac voltage close to the ac pull-in voltage (e.g., 2 V ac) shows ac symmetry breaking (oval shape). Around this ac voltage, M oscillations per period or period M response is observed for an excitation frequency of f_0/M. Figure 3 shows 3 and 7 oscillations per period responses, for a 70 V dc bias at 7 V and 7.17 V ac voltages (both these ac voltages are in the ac symmetry breaking region for 70 V dc), respectively. $f_0 = 0.943$ Mhz at 70 V dc. Up to 8 oscillations per period are observed in the present system.

In order to understand the reason for the formation of M oscillations per period at f_0/M, an analytical mass-spring-damper (MSD) model [5] ($\ddot{x} + 2\zeta\dot{x} + x = F_e/mg\omega_0^2$) for the MEM system is considered. The parameter values are

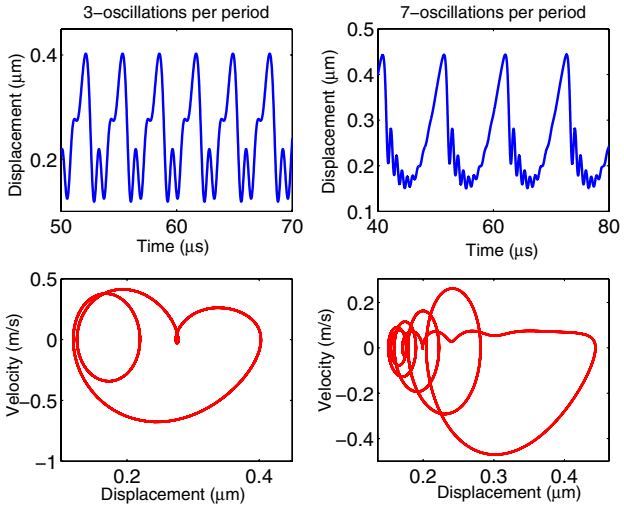

FIG. 3 (color online). Three oscillations per period and seven oscillations per period at $f_0/3$ and $f_0/7$ excitations, respectively.

$\zeta = 0.1009$, $\omega_0 = 1.1981$ MHz, and $m = 1.864 \times 10^{-12}$ kg for the Si fixed-fixed beam MEM device. These parameters have been computed analytically using linearized Reynolds squeeze film damping [11] and Euler's beam theory [12]. The electrostatic force F_e can be written as [13]

$$F_e = \frac{\epsilon A V^2}{2g^2(1-x)^2} = \frac{\epsilon A V^2}{2g^2}[1 + 2x + 3x^2 + 4x^3 + \cdots] \quad (4)$$

where g is the gap in the undeformed state between the microstructure and the ground electrode and A is the area of the microstructure surface facing the ground electrode. The series expansion of F_e indicates that the MSD model is the general form of the Duffing equation [14] having an infinite series of x with time-varying coefficients in the forcing term. The formation of two oscillations per period at $f_0/2$, and three oscillations per period at $f_0/3$, has been shown for the Duffing equation due to the presence of quadratic and cubic terms of the normalized displacement x [14]. The MSD model has even higher-order terms of x from the electrostatic force F_e, which can be attributed for the formation of higher-order oscillations. The MSD model is analyzed using the harmonic balance method [14] to explain the formation of M oscillations per period. Expressing the displacement x as a Fourier series $x = \Sigma_{M=1}^{NT} X_M \exp(jM\omega t)$, a closed form expression for X_M can be obtained. NT is the number of harmonics considered and $\omega = 2\pi f$. Figure 4(a) shows the variation of X_1, X_2, and X_3 with the frequency of excitation. It is observed that the value of X_M peaks at $f = f_0/M$, making the ratio X_M/X_1 maximum at that frequency. This results in the formation of M oscillations per period at $f = f_0/M$ [14]. The formation of M oscillations per period at $f = f_0/M$ takes place through the formation of lower-order oscillations with increasing ac voltage, as can be inferred from

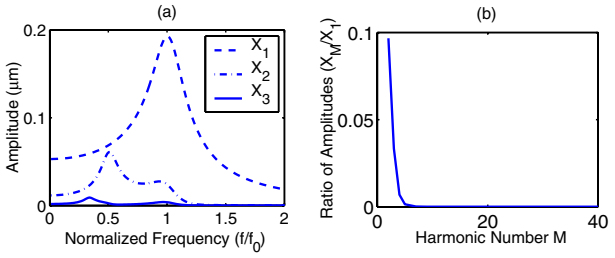

FIG. 4 (color online). (a) Variation of X_1, X_2, and X_3 with excitation frequency. (b) Variation of the ratio of the amplitudes with the harmonic number.

Fig. 4(a). A two oscillation per period response is formed before the emergence of the three oscillation per period response at $f_0/3$ with increasing ac voltage as X_2/X_1 is significant even at smaller ac voltages as opposed to X_3/X_1, which is significant only at higher ac voltages. Similar observations can be made for higher values of M. The absence of very high-order oscillations (large M) can be explained by the fact that the ratio X_M/X_1 decreases rapidly with increasing M as shown in Fig. 4(b). As the formation of the M oscillations per period response can be explained from the MSD model, it can be concluded that the nonlinearity from electrostatics is responsible for the reported observations and not the mechanical and/or the fluidic nonlinearities as these are neglected in the MSD model.

As the ac voltage is increased further beyond the ac symmetry breaking point, a cascade of period doubling bifurcations is observed, resulting in the formation of 2^n M oscillations per period at the excitation frequency of f_0/M. Figure 5 shows a sequence of period doubling bifurcations, $n = 0, 1, 2, 3$ for a three oscillation per period response at $f_0/3$ excitation for increasing ac voltages of 5.9, 5.99, 6.003, and 6.005 V, respectively, at 71 V dc bias ($f_0 =$ 0.885 MHz). A 71 V dc bias is also in the dc symmetry breaking region for the system. The phase plot and the Poincaré map for the chaotic state observed on further increasing the ac voltage to 6.01 V is shown in Fig. 6. The existence of chaos is further validated by the computation of the largest Lyapunov exponent (λ) of the system from the time series data obtained from the numerical simulation using the software package TISEAN [15]. A positive value of $\lambda = 0.09716$ was obtained at 6.01 V ac. A similar set of observations were made for other values of M thereby showing the existence of 2^n M oscillations per period.

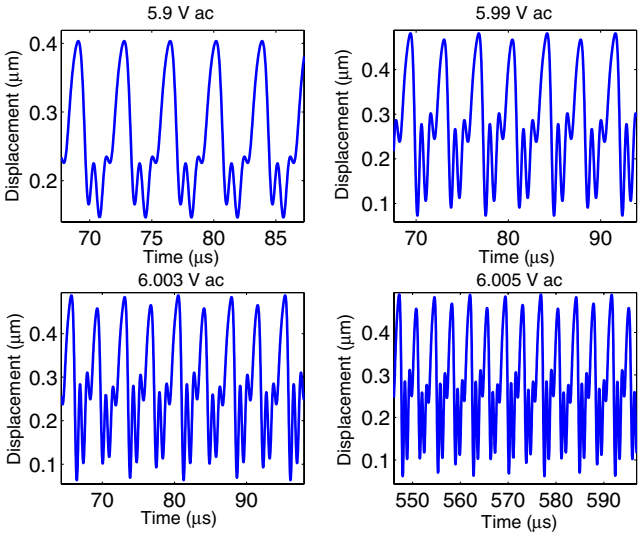

FIG. 5 (color online). Sequence of period doubling bifurcations at $f_0/3$.

Investigations reveal that both dc and ac symmetry breaking are needed for chaos to set in through the period doubling route. At small dc bias, applying a large ac voltage causes ac symmetry breaking but no period doubling and chaos was observed. The MSD model yielded similar observations, indicating electrostatic force as the cause of these period doubling bifurcations and chaos. The development of chaos can be further investigated by studying the behavior of the overall nonlinear force $f(x)$ acting on the microstructure using the MSD model.

$$f(x) = x - \frac{\epsilon A V^2}{2g^3 m\omega_0^2}[2x + 3x^2 + 4x^3 + \cdots]. \quad (5)$$

As the dc voltage is increased (10 to 60 V in steps of 10 V) in the MSD model, $f(x)$ develops a smooth bend in its shape as shown in Fig. 7. The circular markers denote the points where $f'(x) = 0$ (changes from positive to negative). The value of $f(x)$ is computed for the maximum displacement x that is obtained for a combined dc and ac signals. For small dc voltages, where the bend is sharp, the structure becomes unstable as soon as it crosses the $f'(x) =$ 0 point and no period doubling route to chaos is observed. However, it appears that a large dc bias results in the

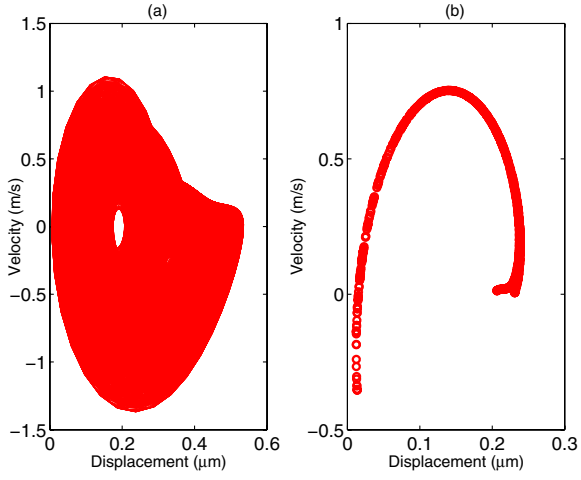

FIG. 6 (color online). (a) Phase plot and (b) Poincaré map for chaos at $f_0/3$.

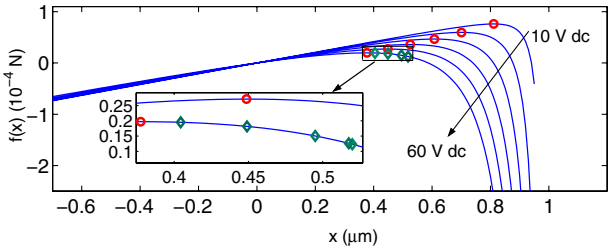

FIG. 7 (color online). Variation of $f(x)$ with dc bias.

formation of a smooth bend in $f(x)$ where the structure is stable for a small region after the $f'(x) = 0$ point. It is observed from Fig. 7 that the period doubling route to chaos is located in this region for such large dc voltages. From Fig. 7, it can be seen that $f(x)$ is more sensitive to x (higher nonlinearity) after the bend and much less sensitive to x (lower nonlinearity) before the bend. This indicates that the system undergoes qualitative changes during the bend formation and goes from a state of less sensitivity on x to a state of high sensitivity on x to instability. As a result, the period doubling bifurcations (qualitative changes in the system) can be expected to be found in the bend region. It is to be noted that a higher voltage (around 70 V dc) was needed in the full scale simulation as compared to 60 V dc in the MSD to observe chaos. This is due to the presence of mechanical and fluid damping nonlinearities in the full scale simulations. The change in the structural stiffness and damping coefficient with deformation gives rise to mechanical and fluidic nonlinearities. They are assumed to be a constant in the MSD model.

The first period doubling bifurcation is found to take place in a chaotic manner in the full scale simulation (this was also observed using the MSD model). Figure 8 shows the formation of period 2 (six oscillations per period) from period 1 (three oscillations per period) in a sequence, with increasing ac voltage (5.9, 5.95, 5.984, and 5.99 V) at $f_0/3$. Period 1 gives rise to a 1-band chaotic attractor, which in turn gives rise to a 2-band chaotic attractor. The 2-band chaos in turn collapses to a stable period 2 orbit. This observation was made for the other superharmonic excitations as well. The first Lyapunov exponent was found to be positive during this period doubling, indicating a chaotic transition.

In conclusion, complex oscillations and chaos under superharmonic excitation and chaotic transition during the first period doubling bifurcation are reported for electrostatic MEMS. dc and ac symmetry breaking and bending of the overall nonlinear force are shown as prerequisites for the reported observations.

This work is supported by the National Science Foundation under Grants No. CCR-0121616 and No. ACI-0217986.

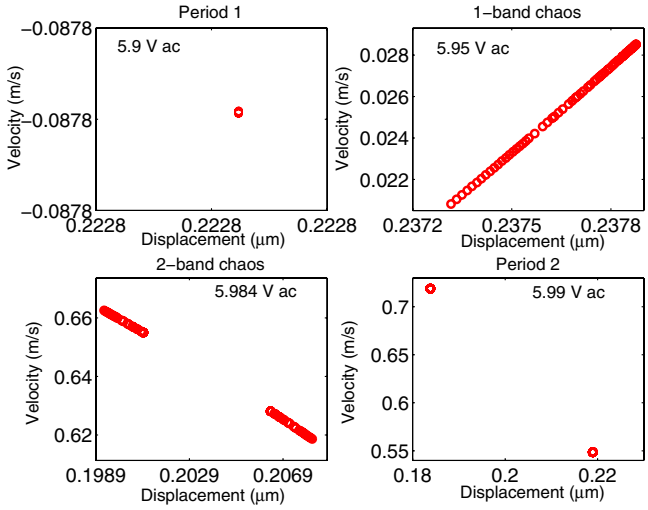

FIG. 8 (color online). Poincaré maps for transition from period 1 to period 2 through 1-band and 2-band chaos.

*Corresponding author: http://www.uiuc.edu/~aluru

[1] S. G. Adams, F. Bertsch, and N. C. MacDonald, in *Proceedings of the Ninth Annual International Workshop on Micro Electro Mechanical Systems, 1996, (MEMS '96)* (IEEE, New York, 1996), p. 32.
[2] J. Bienstman, R. Puers, and J. Vandewalle, in *Proceedings of the Eleventh Annual International Workshop on Micro Electro Mechanical Systems, 1998. (MEMS '98)* (IEEE, New York, 1998), p. 562.
[3] Y. C. Wang, S. G. Adams, J. S. Thorp, N. C. MacDonald, P. Hartwell, and F. Bertsch, IEEE Trans. Circuits Syst. I **45**, 1013 (1998).
[4] C. Gui, R. Legtenberg, H. A. C. Tilmans, J. H. J. Fluitman, and M. Elwenspoek, J. Microelectromech. Syst. **7**, 122 (1998).
[5] S. Liu, A. Davidson, and Q. Lin, in *Proceedings of the 12th International Conference on Solid-State Sensors, Actuators and Microsystems, 2003* (IEEE, New York, 2003) vol. 2, p. 1092.
[6] J. D. Jackson, *Classical Electrodynamics* (John Wiley & Sons, New York, 1999).
[7] G. Li and N. R. Aluru, IEEE Trans. Comput.-Aided Des. Integr. Circuits Syst. **22**, 1228 (2003).
[8] A. Burgdorfer, J. Basic Eng. **81**, 94 (1959).
[9] S. K. De and N. R. Aluru, J. Microelectromech. Syst. **13**, 737 (2004).
[10] U. Parlitz and W. Lauterborn, Phys. Lett. **107A**, 351 (1985).
[11] J. M. Huang, K. M. Liew, C. H. Wong, S. Rajendran, M. J. Tan, and A. Liu, Sens. Actuators A, Phys. **93**, 273 (2001).
[12] E. G. Popov, *Engineering Mechanics of Solids* (Prentice-Hall, Englewood Cliffs, NJ, 1997).
[13] M. I. Younis, E. M. Abdel-Rahman, and A. Nayfeh, J. Microelectromech. Syst. **12**, 672 (2003).
[14] A. T. Nayfeh and D. T. Mook, *Nonlinear Oscillations* (John Wiley & Sons, New York, 1979).
[15] R. Hegger, H. Knatz, and T. Schreiber, Chaos **9**, 413 (1999).